R-06-25

Effect of single-fracture aperture variability on field-scale transport

Scott Painter
Center for Nuclear Waste Regulatory Analyses
Southwest Research Institute®

January 2006

Svensk Kärnbränslehantering AB
Swedish Nuclear Fuel
and Waste Management Co
Box 5864
SE-102 40 Stockholm Sweden
Tel 08-459 84 00
+46 8 459 84 00
Fax 08-661 57 19
+46 8 661 57 19

ISSN 1402-3091
SKB Rapport R-06-25

Effect of single-fracture aperture variability on field-scale transport

Scott Painter
Center for Nuclear Waste Regulatory Analyses
Southwest Research Institute®

January 2006

Contents

1 Introduction

The role of the flow-dependent parameters τ [T] and β [T/L] in controlling transport and retention in heterogeneous fractures and fracture networks was established in previous SKB projects /e.g. Cvetkovic et al. 1999, 2004, Painter et al. 1998/. The non-reacting travel time τ [T] and cumulative reactivity parameter β [T/L] (also referred to as transport resistance and denoted F) are cumulative parameters obtained by integrating along random streamlines. Once the probability distributions for these parameters are known, probabilistic simulations of transport can be performed with relatively little effort.

Detailed analyses /Cvetkovic et al. 2004/ of comprehensive discrete-fracture network simulations using the FracMan platform /Outters 2003/ clearly demonstrate that the distributions of τ and β are highly non-Gaussian at the scales of interest, which is inconsistent with the results of continuum models and suggests that discrete fracture network (DFN) simulation is a more reliable method for assessing transport in sparsely fractured rock. However, DFN simulations are computationally expensive, and usually limited to relatively small scales. To overcome this limitation, a method /Painter and Cvetkovic 2005/ for direct upscaling of discrete fracture networks was developed in previous SKB projects. The upscaling method allows results from relatively small-scale DFN simulations to be used in probabilistic simulations at the field scale.

To be accurate, any DFN-based simulation must adequately represent the transport processes at small scales. Aperture variability within individual fractures is routinely neglected in DFN simulations. That is, individual fractures are assumed to be homogeneous. The cumulative reactivity parameter β is then computed as a ratio of the "flow-wetted surface" and flow rate of an individual fracture. In reality, individual fractures are heterogeneous, which may cause flow to be "channelized" in individual fractures. However, the importance of internal variability relative to other sources of variability in the flow system is not obvious. On the one hand, internal variability in aperture tends to be smaller than fracture-to-fracture variability, which would suggest that internal aperture variability is less important. On the other hand, flow channeling in heterogeneous fractures tends to cause flow lines to coalesce in high-velocity regions, which may introduce a systematic bias toward lower β and less retention.

Previous studies /Cvetkovic et al. 1999/ of the transport effects of flow channeling in variable-aperture fractures typically considered a single fracture isolated from the rest of the network. Although these studies yield some clear insights into the process, the unrealistic boundary conditions for flow limit the usefulness of the results for field-scale applications. Flow in an individual fracture is controlled not only by the aperture variability, but also by the boundary conditions that are determined by connections with other fractures in the network. Fluid may enter and leave a fracture only where the fracture intersects other fractures. These connections may represent a relatively small fraction of the fracture surface. This limited connection to other fractures introduces a certain degree of flow channeling independent of that caused by aperture variability. The relative importance of the two channeling mechanisms – heterogeneity-induced or geometry-induced – cannot be investigated without considering heterogeneous fractures embedded in a three-dimensional network.

The effects of within-fracture variability relative to those of fracture-to-fracture variability were investigated previously by /Painter and Cvetkovic 2001/. The conclusion from that study was that within-fracture aperture variability contributes little to field-scale transport because it is overwhelmed by the much larger fracture-to-fracture variability. However, that

study used a kinematic representation of the streamline that did not explicitly resolve flow dynamics within the fracture. The consequences of this approximation are not clear, which leaves the issue of internal variability unresolved.

This report addresses the importance of internal fracture aperture variability in determining field-scale transport in fractured rock. Discrete fracture network simulation with internal aperture variability within each fracture is the primary tool for the investigation. This approach makes it possible to investigate the relative importance of the various sources of flow channeling and their effect on field-scale transport.

2 Methods and procedures

DFN simulation and particle tracking were the primary tools for this study. Networks of 30–50 randomly placed fractures were simulated. Aperture variations within each fracture were modeled as random space functions, and simulated using stochastic simulation methods. After simulating the fracture network, Laplace's equation was solved to establish the steady-state flow field. Particle tracking in the steady-state velocity field was then used to calculate random trajectories and the associated τ and β parameters. The set of the calculated τ and β represent a random sample from the underlying joint distribution. By comparing the calculated sample distribution for various degrees of assumed internal aperture variability it is possible to quantify the effect of aperture variability.

DFN simulation is a standard approach for investigating transport in sparsely or moderately fractured rock. However, particle tracking within three-dimensional DFNs is difficult to implement accurately. Numerical implementation of particle tracking in two-dimensional single fractures or fully three-dimensional aquifers is well understood. In three-dimensional DFNs, however, particles move in a random velocity field that is intermediate between two-dimensional and three-dimensional. Within a single fracture, the velocity field is two-dimensional, but at fracture intersections three-dimensional effects, which cause mass transfer between fractures, must be accounted for. Although conceptually straightforward, this intermediate situation is numerically delicate and appears to be susceptible to numerical artifacts. Significant numerical artifacts have been identified /Painter 2003/ in standard commercial software. To avoid these numerical artifacts, an approximate, but more robust, simulation approach was developed. This alternative simulation method is based on particles that "hop" from node to node on a regular finite-difference grid.

Details of the simulation procedure and the node-routing particle transport method are provided in the following subsections.

2.1 Simulation procedure

The numerical experiments used the following procedure.

1. A realization of the DFN was created by sampling from pre-specified distributions of log-transmissivity for disk-shaped fractures. Log-transmissivity in this context refers to an average value for the individual fracture.
2. For each fracture in the network, a random field with zero mean and unit variance was generated by stochastic simulation. The random fields were saved.
3. A log-transmissivity field for each fracture was created by scaling its random field by σ and adding the result to the average value from Step 1. Here σ^2 is the log-variance for internal variability. The result was then exponentiated to obtain a transmissivity field. Aperture was calculated from transmissivity using the quadratic law.
4. Step 3 was repeated for different values of the parameter, σ, representing different heterogeneity levels. Four values of σ^2 were used: 0, 1, 2, and 3. Thus, each realization of the DFN from Step 1 spawned four DFN realizations with internal aperture variability and different levels of heterogeneity.
5. Flow fields, particle trajectories, and resulting τ,β distributions were generated for each of the four realizations in Step 4.

Steps 1–3 create a hierarchical random field for the transmissivity; the geometric mean transmissivity varies from fracture to fracture, and the local transmissivity within each fracture varies spatially around its geometric mean.

The four realizations created in Step 4 are perfectly correlated but with different levels of heterogeneity. This correlated sampling procedure prevents random fluctuations from obscuring any heterogeneity-induced effects on the τ,β distribution, thus allowing meaningful results to be extracted from a relatively small number of realizations.

The 5-step procedure was repeated to create 10 independent realizations of the DFN. Because each independent realization results in 4 correlated realizations, the particle tracking calculation (Step 5) was performed on 40 realizations for each combination of input parameters.

2.2 Lattice representation of the DFN

A lattice-based approach similar to the smeared-fracture model /Svensson 2001/ was used to represent the DFN and the velocity field. In the particular variant used here, the simulation domain was first subdivided into a large number of rectangular cells. If a simulated fracture intersected the face between two adjacent cells the link between those two cells was activated and assigned the transmissivity of the fracture. If a cell face was not intersected by a fracture, the link between the adjacent cells remained inactive. Repeating the procedure for all fractures in the DFN resulted in a sparse lattice network of short pipe segments (links or bonds) representing the DFN (see Figure 2-1). Internal variability in fracture transmissivity and aperture is easily incorporated – the transmissivities of the bonds representing each fracture was assigned by stochastic simulation, as described later in this report. Steady-state hydraulic head on the lattice was solved by applying Kirchoff's law to each node. A sparse linear solver was then used to solve the resulting linear system. /Svensson 2001/ used detailed numerical simulation to investigate the accuracy of the closely related smeared fracture model, and demonstrated that the method is accurate provided the cell size is sufficiently small.

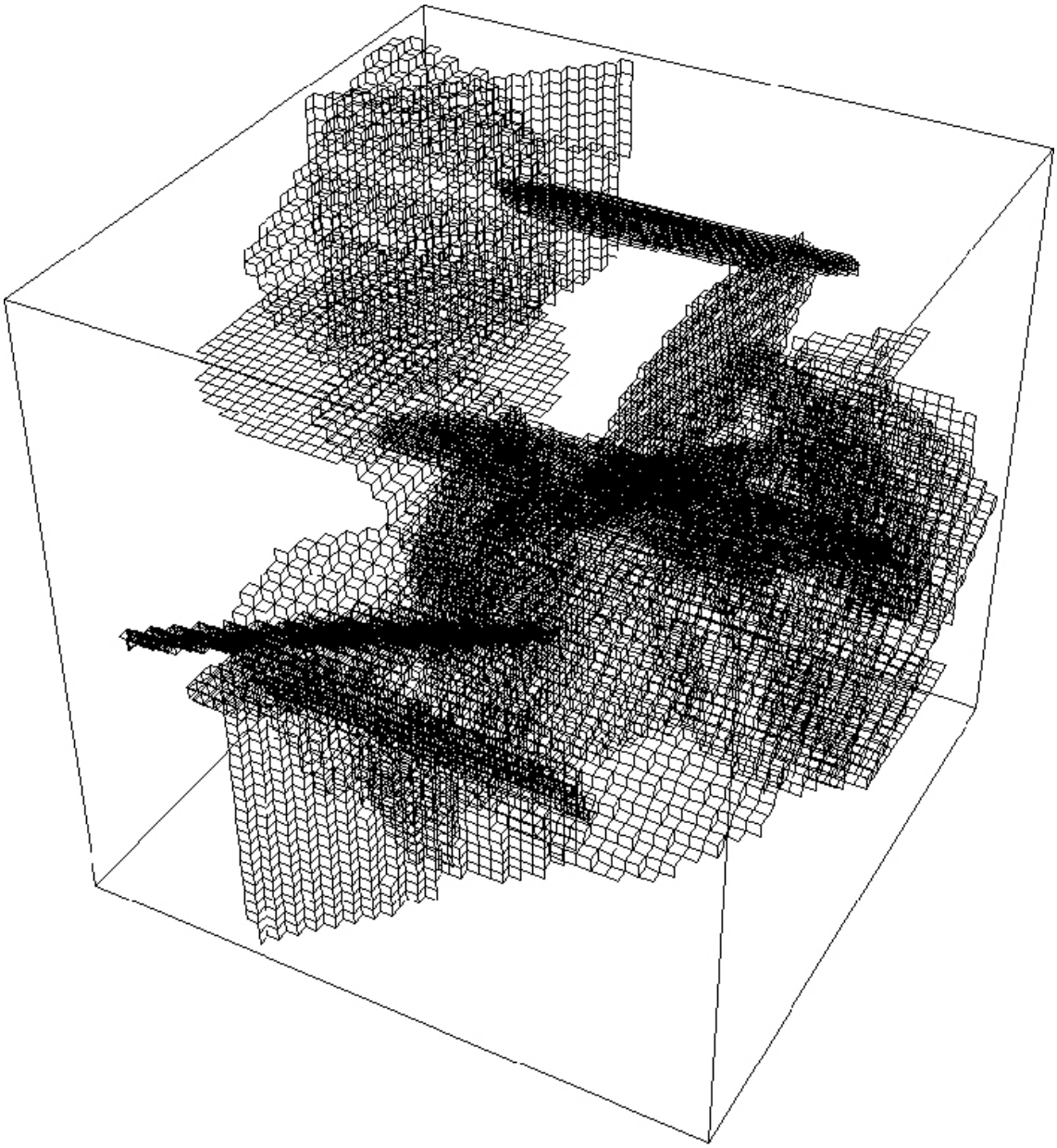

Figure 2-1. *Example pipe network resulting from the lattice-based representation of a DFN.*

2.3 Node-routing method for particle transport

Once the hydraulic head on the lattice network representing the DFN has been established, the next step was to move particles through the lattice network and accumulate statistics on τ and β. A node routing method was developed to mimic purely advective movement within a fracture and complete mixing at fracture intersections. In this method, a particle hops from node to neighboring node. If the starting node belongs to only one fracture, then the particle moves to a downstream node along the link (pipe segment) with the largest outgoing flux. This choice is intended to mimic purely advective transport within single fractures. If the starting node belongs to multiple fractures, then the particle is moved along a link selected randomly from the links with outgoing flux. The probability for selecting a given link in this case is weighted by the magnitude of the outgoing flux, thus mimicking complete mixing at

fracture intersections. The residence time (and hence incremental increase in τ) in the link connecting the two nodes is determined by the flow velocity in that link. Similarly, the incremental increase in β is determined by the flow velocity and fracture aperture of the link.

If the local velocity field is aligned with the regular lattice network, then the node routing approach provides an exact representation of the trajectory and the associated τ and β. If the velocity is misaligned from the lattice principal direction by 45°, then the simulated trajectory will oscillate in step-wise manner around the true trajectory and the travel distance will be overestimated by a factor of $\sqrt{2}$. In addition, the flow velocity will be underestimated by the same factor, with the net effect being to overestimate τ and β by a factor of 2. A heuristic correction is used to compensate for this bias in the estimated flow-dependent transport parameters. The heuristic correction is calculated by first finding the true flow direction as the resultant of the link velocities. The angle θ between the true flow direction and the selected link direction is then calculated. The incremental increase in τ and β along the link is then decreased by a factor of $\cos^2(\theta)$. This correction exactly compensates the bias if the lattice principal direction and flow direction are misaligned by 45° and has no effect if the lattice principal direction and flow direction are aligned. Note that the procedure works on arbitrary unstructured grids, but is applied only to regular structured grids in this report.

Although the particular variant of the node-routing method developed for this study appears to be new, the method is related to the node-routing scheme used by /Desbarats 1990/ in his well-known study of transport in sand/shale sequences. The new aspects of the node-routing method developed for this study are the deterministic routing within individual fractures, the correction to remove the systematic bias in the trajectory lengths, and the validation efforts. Performance assessment calculations for the potential repository at Yucca Mountain, Nevada also use a particular type of node-routing scheme /Robinson et al. 2003/. Their "cell-based particle tracking" method included strong retention processes and was tested against alternative modeling approaches.

Numerical experiments were used to test the accuracy of the lattice hopping method. The scenario for the test was a single horizontal fracture placed at the horizontal midplane of a simulation volume. The fracture diameter is large compared to the domain size, thus generating a fully two-dimensional pathway from the upstream to downstream sides of the volume. The SGSIM code from GSLIB /Deutsch and Journel 1992/ was used to simulate three realizations of the transmissivity field for the fracture. The log-normal random space function model was used, with log-variance of 0.1, 1 and 3 for the three realizations of transmissivity. Aperture was calculated from transmissivity using a quadratic law /Outters 2003/. A macroscopic hydraulic gradient was applied in one direction, with no-flow boundary conditions on the other sides. Because the flow path and resulting velocity field were fully two-dimensional, conventional particle tracking is straightforward, thus providing an independent benchmark solution. Particles were released on the upstream side and moved through the velocity field by conventional particle tracking and by the node-hopping method.

Particle trajectories obtained from the conventional particle tracking and the node-hopping method are shown in Figure 2-2 for the test case with log-variance of 3. The particle trajectories, which are initially distributed across the upstream end of the fracture, tend to coalesce into a small number of relatively thin flowing zones as they move through the fracture. This general behavior is reproduced in the node-routing results. More importantly, the τ and β distributions obtained from the node-routing method are in close agreement with the conventional particle tracking results. Distributions of β as calculated by the two methods are compared in Figure 2-3. The test case with log-variance of 1 is shown in Figure 2-3a, and the more heterogeneous case with log-variance of 3 is shown in

Figure 2-3b. In both cases, the difference between the conventional particle tracking and the node routing results is much smaller than the spread in the distribution. Similar results (not shown) were obtained for the τ distributions and for the weak heterogeneity case. These successful tests demonstrate that the node-routing method is adequate for the purposes of this study.

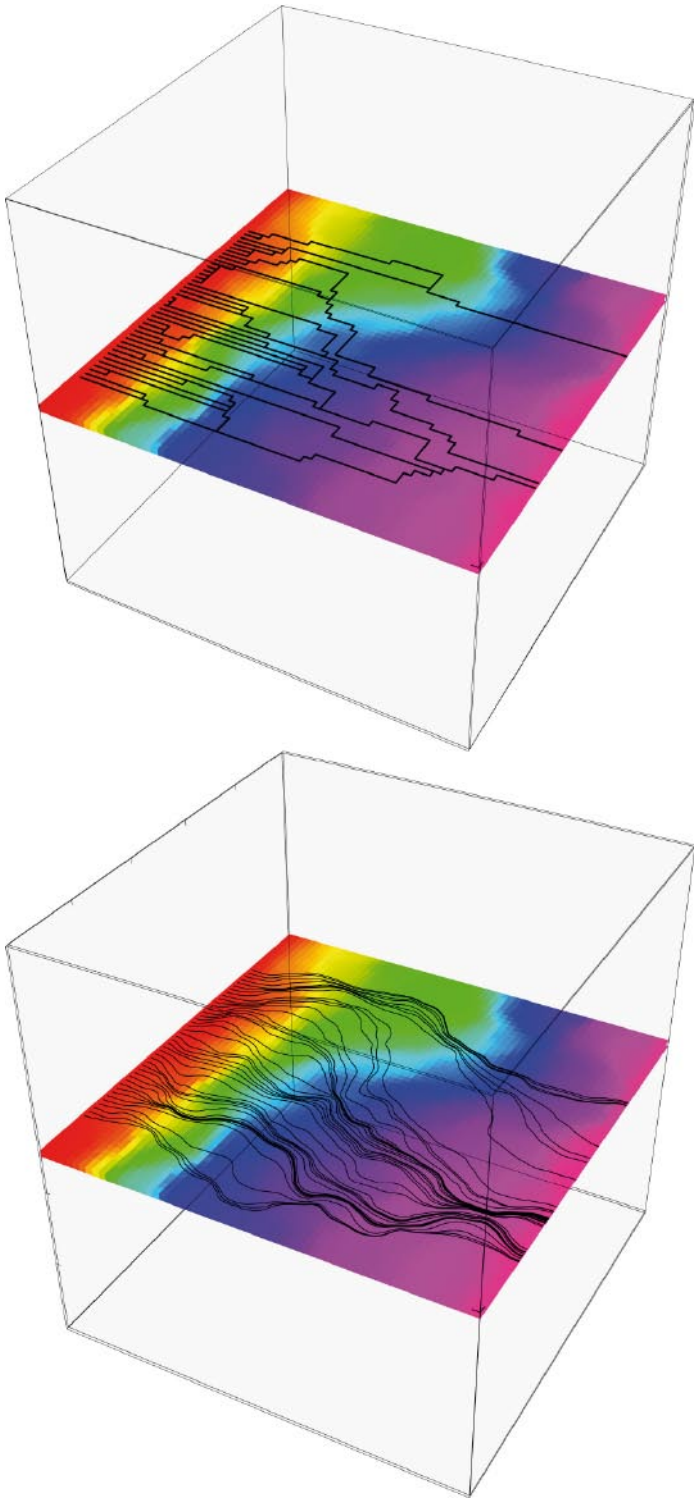

Figure 2-2. *Single-fracture configuration used to test the accuracy of the node-routing scheme used in this report. Flow is from left to right. The hydraulic head on the single fracture is shown in color. Particle tracks obtained from the node routing (top) and conventional particle tracking (bottom) are also shown.*

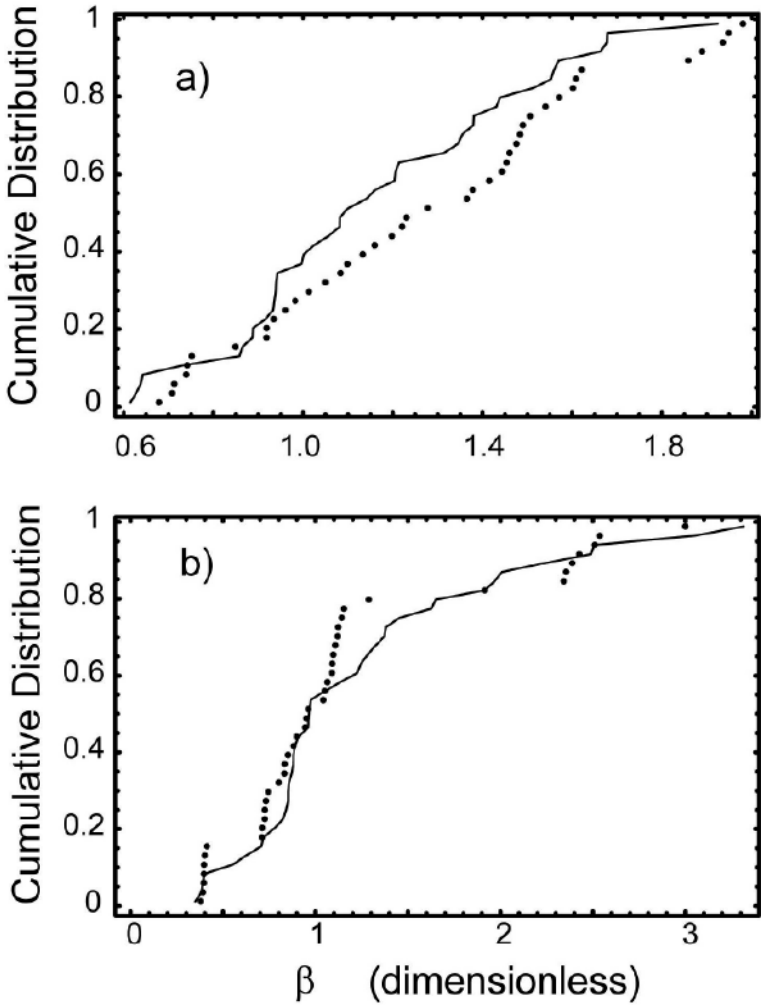

Figure 2-3. *Comparison of calculated cumulative reactive distribution based on traditional particle tracking (solid curves) and node-routing scheme (individual data points) on a single-fracture with low (a) and high (b) variability.*

2.4 Single-fracture transmissivity simulation

The transmissivity fields for the individual fractures were generated by geostatistical stochastic simulation. This process requires a random space function (RSF) model for the transmissivity variations.

/Brown 1995/ measured surface profiles of several natural fractures, and found that surface roughness is accurately represented by self-affine fractal models that lack a characteristic length scale. However, long wavelength variations in the two surfaces of each fracture are closely correlated, which introduces a wavelength cutoff in the aperture variability. Aperture variation in this situation is consistent with a conventional geostatistical model with a single correlation length.

Mapped distributions of void space in natural fractures subject to applied stress generally show increasing contact area with increasing stress (Gale 2005). (Gale 2005) used the resin impregnation method to characterize the void-space geometry of several natural granite fractures subject to known stress, and found that the aperture distribution in the open part of the fracture is well approximated by a log-normal distribution.

Asperities were neglected in this study and aperture was modeled as having a log-normal distribution. The log-normal model for aperture is widely used in studies of transport in fractured rock, and is an appropriate first approximation for studying the relative effects of internal aperture variability.

If aperture b and transmissivity T are related as $T \propto b^a$, as is typically assumed, then a log-normal distribution of aperture implies a log-normal distribution of transmissivity, albeit with different distribution parameters. For a parallel plate model, a is equal to 3 (cubic law). A quadratic law ($a = 2$) sometimes provides a better fit to field data /Doe 1993/ and was used in this study.

Log-transmissivity variation within individual fractures was modeled as a conventional multi-normal random-space function with an exponentially decaying autocorrelation. The sequential Gaussian simulation code SGSIM from the GSLIB collection was used to generate the transmissivity fields.

3 Transport effects of fracture aperture variability

3.1 Parameters for the reference case and variants

Five sets of simulations were performed. The domain for each was 12×12×12 m in size and was subdivided into 81×81×81 computational cells. Ten realizations of the DFN were generated for each set. As described previously in this report, four simulations corresponding to different levels of internal variability were performed for each realization of the DFN. For each simulation, 500 particles were tracked. A flux-weighted particle source was used; that is, the probability for picking one of the cells on the upstream face of the domain as a starting point was proportional to the flux through that location.

Networks of 35 fractures were simulated for the reference case. Fracture radius was selected from a log-normal distribution with geometric mean of 3.5 m and log-variance of 0.3. Fracture orientation was random and isotropic. Fracture transmissivity (spatial average for fracture) was log-normal with log-variance of 1. The log-normal RSF model with correlation length (isotropic) of 2 m was used to model the internal transmissivity variability.

Five variant cases were considered:

- Case HD has a higher fracture density than the reference case. In this case 50 fractures were simulated in each DFN. Other parameters are the same as the reference case.
- Case LC has a longer correlation length (4 m), but is otherwise identical to the reference case.
- Case SC has a shorter correlation length (1 m), but is otherwise identical to the reference case.
- Case RV has reduced fracture-to-fracture variability in transmissivity. A log-variance of 0.0025 was used instead of the reference-case value of 1.
- Case RI is identical to the reference case except that a residence injection source is used instead of the flux-weighted source.

3.2 Reference case results

Calculated hydraulic head for one realization from the reference case is shown in Figure 3-1. Flow is from left to right in this case. Note the unequal distribution of hydraulic head in the network. Particle tracks for the same realization are shown in Figure 3-2.

Distributions of τ for the four levels of heterogeneity are shown in Figure 3-3a. The cumulative distribution and complementary cumulative distribution are both shown on a log-log scale to make both tails of the distribution visible. In this and the following figures, τ is shown in arbitrary, but internally consistent, units. Specifically, τ is normalized by the median of the $\sigma^2 = 0$ result. It can be seen from Figure 3-3a, that heterogeneity has no significant effect on the τ distribution.

Distributions of β are shown in Figure 3-3b. The $\sigma^2 = 1$ situation is not significantly different from the $\sigma^2 = 0$ case. For larger values of log-variance, internal heterogeneity causes a shift in the distribution to smaller values. However, the effect is modest and is only significant in the left tail of the distribution. In the $\sigma^2 = 2$ situation, the 0.1 percentile is approximately half of the corresponding percentile in the no-internal variability case ($\sigma^2 = 0$). For larger percentiles, the shift is even smaller: the median β with $\sigma^2 = 2$ is 0.85 of that of the $\sigma^2 = 0$ situation.

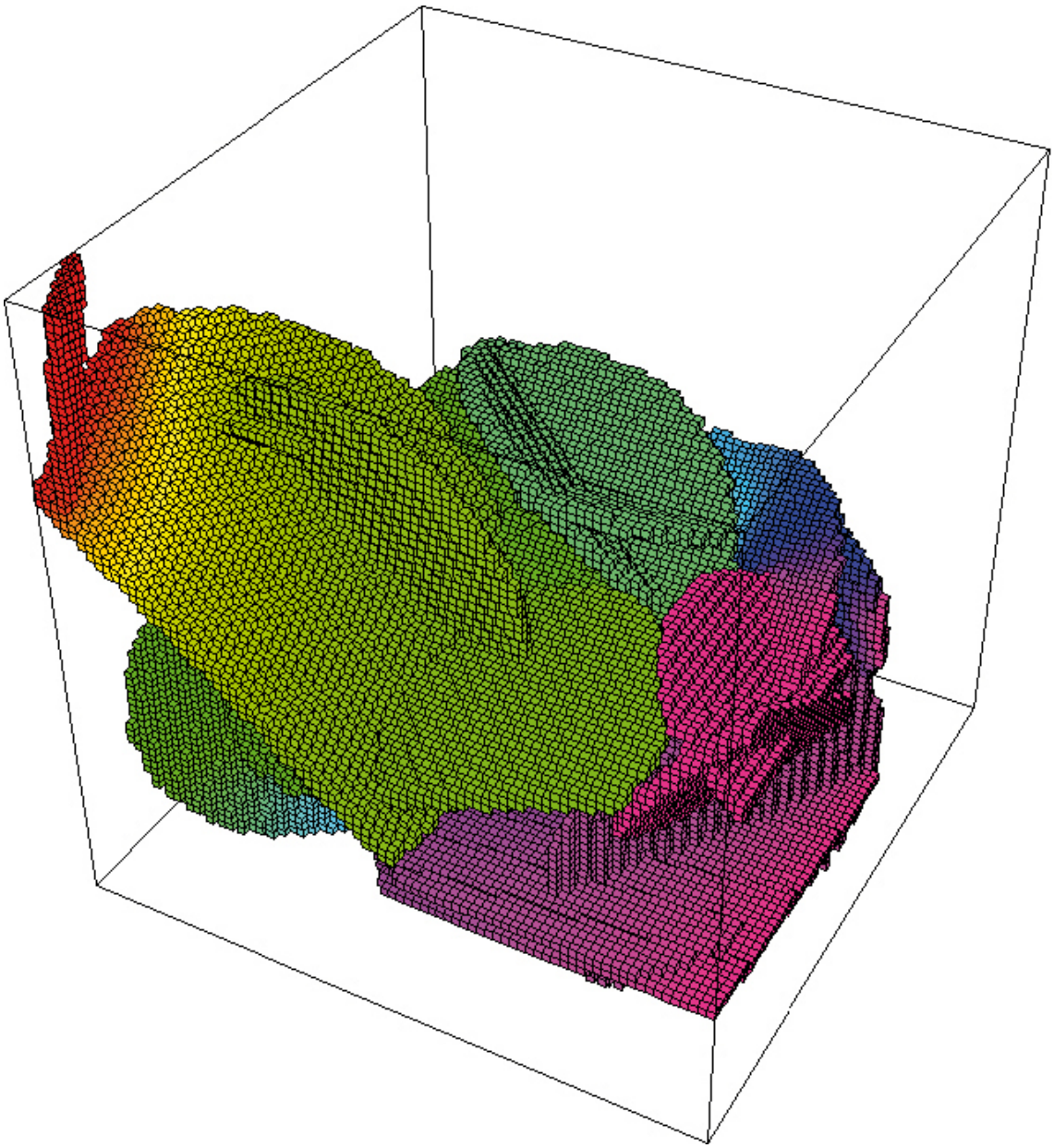

Figure 3-1. *Calculated hydraulic head from one discrete fracture network realization from the reference case set. Flow is from left to right.*

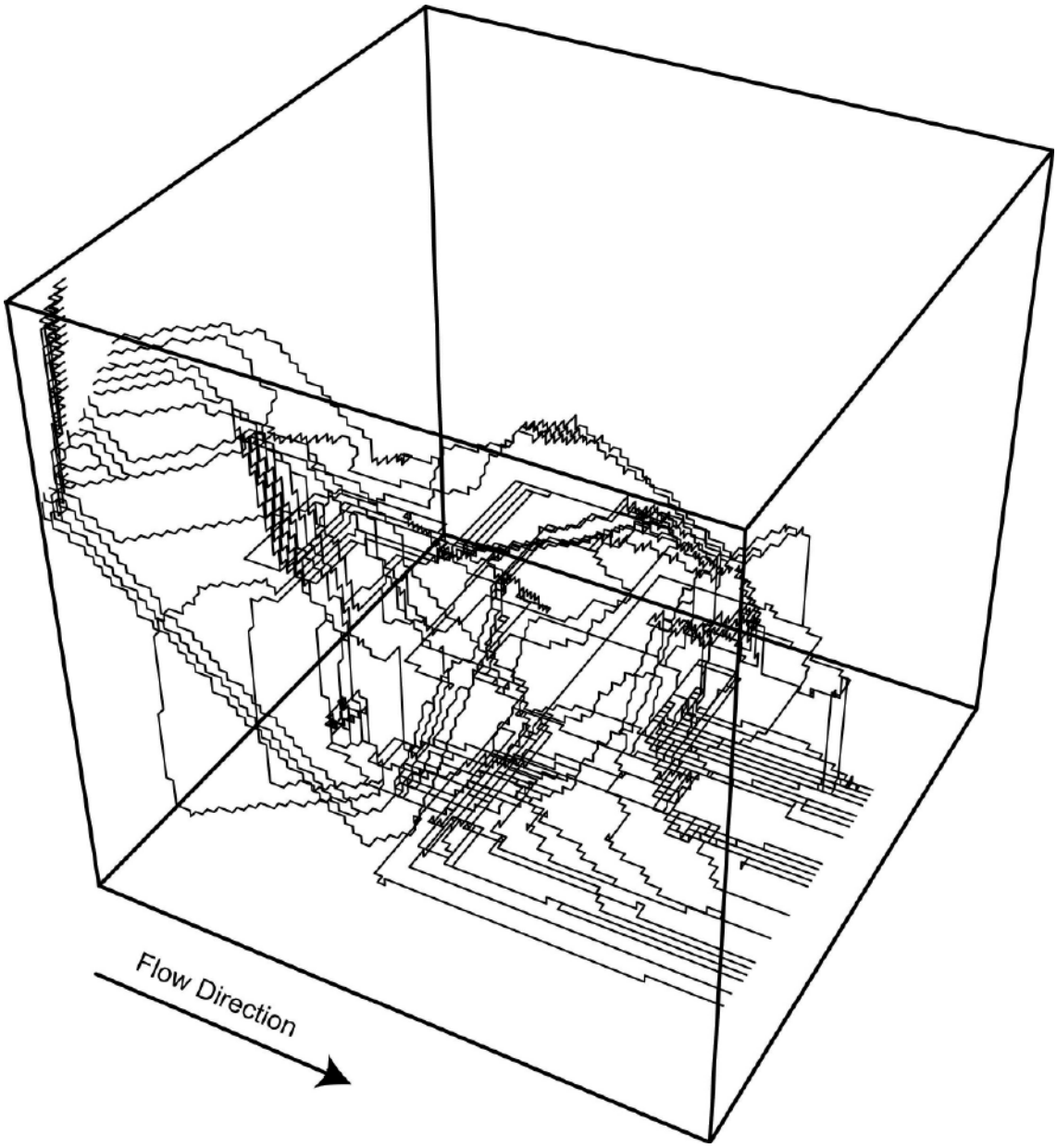

Figure 3-2. *Example particle trajectories obtained by applying the node-routing scheme to the DFN of Figure 3-1.*

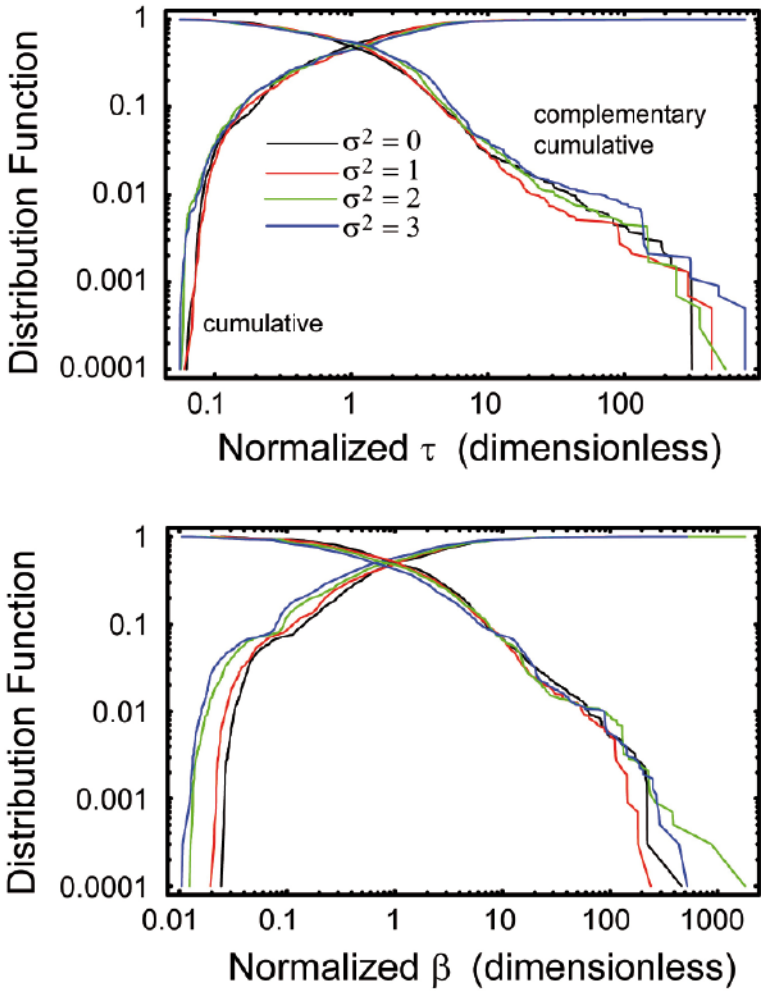

Figure 3-3. *Cumulative and complementary cumulative distributions of τ (top) and β (bottom) for the reference case. The four colors correspond to different levels of internal variability in transmissivity as quantified by the log-variance (σ^2).*

3.3 Parameter sensitivity

For all cases examined, internal heterogeneity had no significant effect on the τ distribution. For that reason, only β results are shown in this section.

Distributions of β for the higher fracture density case (Case HD) are shown in Figure 3-4. The small β tail of the distribution, which is an important control on transport, is affected by heterogeneity in a manner similar to the reference case. However, the effect is somewhat reduced relative to the reference case. The large β tail is more sensitive to heterogeneity. However, the large β tail is relatively unimportant for transport. Moreover, the effect is to shift the distributions to higher values of β, implying reduced transport. Thus, it is conservative from a safety assessment perspective to simply ignore the effect on the large β tail.

Distributions of β for the longer correlation (Case LC) and shorter correlation (Case SC) cases are shown in Figures 3-5 and 3-6, respectively. For both cases, the effect of heterogeneity on the small β tail is similar to that of the reference case. However, the effect is reduced somewhat compared to the reference case.

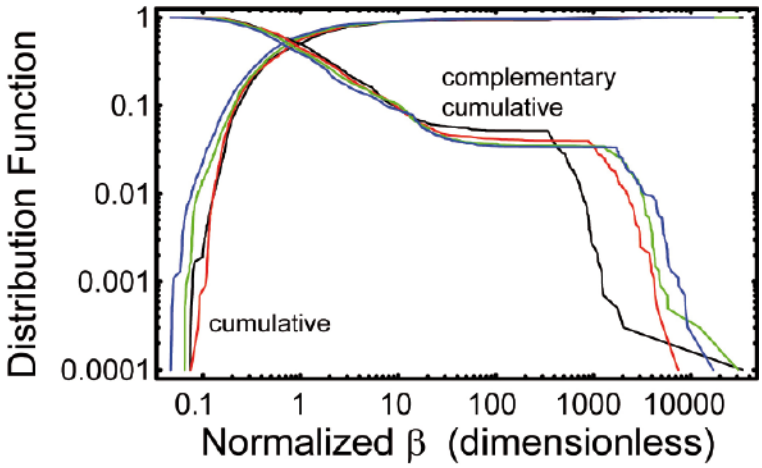

Figure 3-4. *Cumulative and complementary cumulative distributions of β for the Case HD (higher fracture density). The four colors correspond to different levels of internal variability in transmissivity as quantified by the log-variance (σ^2), as in Figure 3-3.*

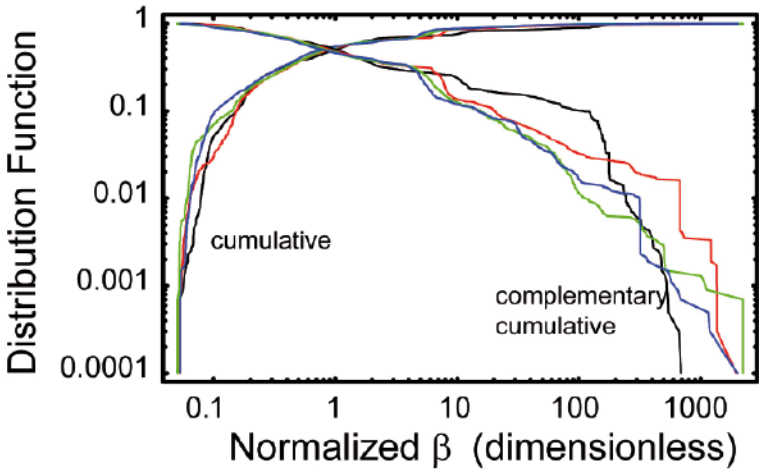

Figure 3-5. *Cumulative and complementary cumulative distributions of β for the Case LC (longer correlation length). The four colors correspond to different levels of internal variability in transmissivity as quantified by the log-variance (σ^2), as in Figure 3-3.*

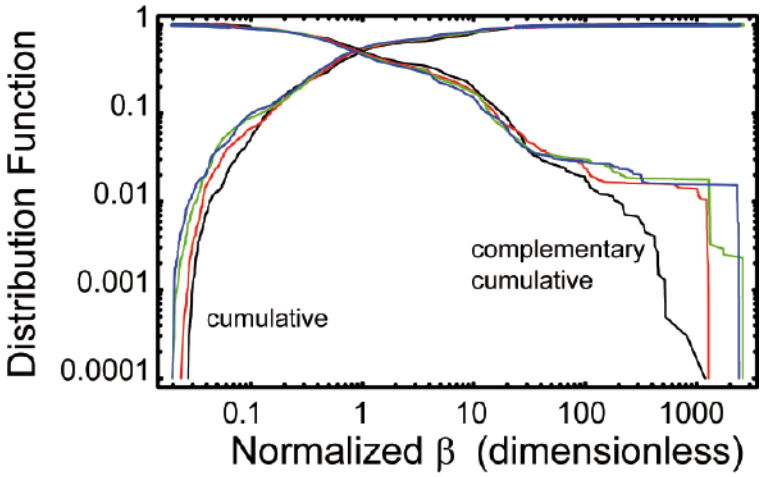

Figure 3-6. *Cumulative and complementary cumulative distributions of β for the Case SC (shorter correlation length). The four colors correspond to different levels of internal variability in transmissivity as quantified by the log-variance (σ^2), as in Figure 3-3.*

Results for Case RV (reduced fracture-to-fracture variability) are shown in Figure 3-7. For this case, internal variability has a greater effect on the β distribution. Specifically, the shift in the small β tail starts at smaller values of σ^2, as opposed to the reference case, which requires a threshold value of σ^2 be reached before internal heterogeneity starts to shift the distribution. A comparison between the reference case and Case RV lends support to the observation that internal variability must exceed fracture-to-fracture variability before internal variability starts to affect the β distribution. Note that Case RV has unrealistically low fracture-to-fracture variability and should not be considered representative of expected conditions.

Results for Case RI (residence injection) are shown in Figure 3-8. The β distribution is broader in the residence injection case and internal variability has an even smaller effect. In fact, no significant effect on the β distribution can be seen in the residence injection case. It is to be expected that the flux weighted injection would result in larger effect of internal variability, because the starting locations with significantly higher fluxes receive comparatively larger number of particles with flux weighted injection, which tends to amplify the effects of internal variability. However, if the simulations are sufficiently large, it is also expected that the flux-weighted and residence injections would start to converge. That is, with larger simulations, the residence injection and flux-weighted cases are expected to become closer, but the flux-weighted case should always result in greater effect of internal variability. In either case, the effect of internal variability on β appears to be modest.

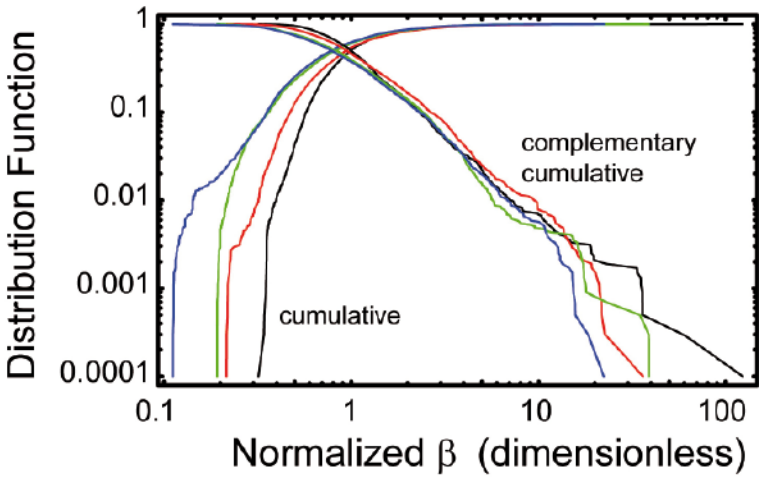

Figure 3-7. *Cumulative and complementary cumulative distributions of* β *for the Case RV (reduced fracture-to-fracture variability). The four colors correspond to different levels of internal variability in transmissivity as quantified by the log-variance* (σ^2)*, as in Figure 3-3.*

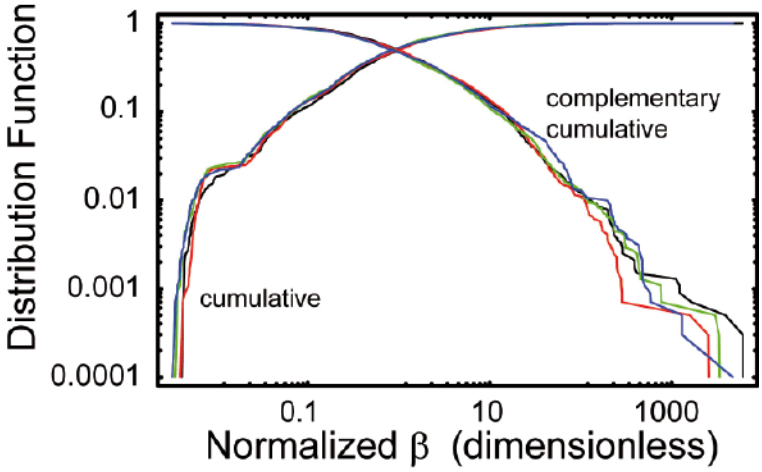

Figure 3-8. *Cumulative and complementary cumulative distributions of* β *for the Case RI (residence injection). The four colors correspond to different levels of internal variability in transmissivity as quantified by the log-variance* (σ^2)*, as in Figure 3-3.*

4 Accounting for internal variability in large-scale DFN simulations

The relatively small effect of internal variability on the cumulative reactivity distribution observed for relevant ranges of parameters suggests a simple scheme for accounting for internal variability in large-scale DFN simulations. The idea is to use small-scale simulations similar to those summarized in Section 3 to define an empirical transformation of the cumulative reactivity distribution. Large-scale DFN simulations without internal variability would then be performed. The results of these large-scale DFN simulations could then be post-processed using the empirical transformation before the results are used in safety assessment. Given that transport results are most sensitive to the left tail of the β distribution and that internal variability does not significantly affect the right tail of the distribution, the transformation need only be applied to the left side of the distribution. Effect of internal variability on the τ distribution was found to be negligible in all cases and can be ignored.

Exploring this idea further, let q_{*p} denote the p-th quantile of cumulative reactivity with internal variability as calculated from small-scale DFNs. The quantile is formally defined as the solution q_{*p} of $F_*(q_{*p}) = p$ where F_* is the distribution function. In addition, let $\overline{q}_{*p}$ denote the corresponding quantity without internal variability. These quantiles can be estimated from small DFN simulations similar to those summarized in this report. An empirical ratio function $\zeta(p) \equiv \frac{q_{*p}}{\overline{q}_{*p}}$ can then be fitted.

Now, let q_p and $\overline{q}_{*p}$ denote p-th quantiles of cumulative reactivity parameter at the larger scale with and without internal variability. The quantiles q_p define the cumulative reactivity distribution at large scales including internal variability at the single-fracture scale, and can be calculated from

$$q_p = \zeta(p)\overline{q}_p \tag{1}$$

Thus, with this procedure, the cumulative reactivity distribution at large scales including the effect of internal variability is obtained.

For the reference case simulations, $\zeta(p)$ can be relatively well fit by

$$\zeta(p) = 0.55 + 0.9p \tag{2}$$

A check on the accuracy of this fit is shown in Figure 4-1. The curve was obtained by applying Equations 1 and 2 to the $\sigma^2 = 0$ results. That is, the case without internal variability was transformed according to the Equations 1 and 2, to obtain the curve in Figure 4-1. This calculation corresponds to how the empirical adjustment might be used in practice once an empirical transform is developed from small-scale DFN simulations. As a check on the accuracy of that procedure, the individual data points representing the distribution obtained from DFN simulations with internal variability ($\sigma^2 = 2$) are also plotted in Figure 4-1. The agreement is very good except in the extreme left tail of the distribution, where the reconstructed distribution is shifted slightly to larger values. This general agreement indicates that the suggested procedure is sufficiently accurate for use in performance assessment studies. However, the empirical transform Equation 2 was developed for a particular combination of DFN parameters and should be revised in applications involving other DFN models.

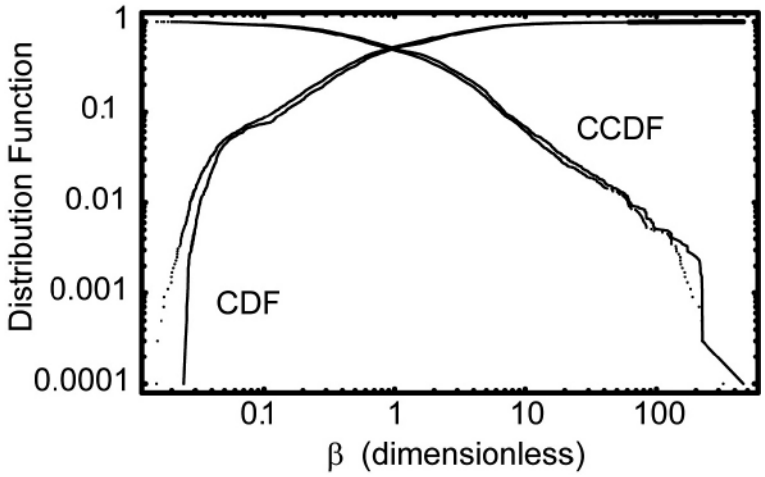

Figure 4-1. *Test of a method for post-processing DFN results to account for internal variability, as described in Section 4. The solid curves are cumulative and complementary cumulative distributions of* β *from DFN simulations with internal variability. The data points represent the same distributions as calculated by post-processing of DFN simulations without variability.*

5 Conclusions and recommendations

The following conclusions can be drawn from the simulations results.

1. Internal variability in aperture and transmissivity causes no significant change in the τ distribution.
2. Internal aperture/transmissivity variability can decrease the cumulative reactivity parameter β, but only when the internal variability equals or exceeds the fracture-to-fracture variability.
3. The decrease in β caused by internal variability is modest. At the leading edge of the distribution, internal variability reduces β by about 50%. In other words, neglect of internal variability would result in about a factor of 2 error in β at the leading edge of the distribution. The reduction is even smaller (~ 15%) in the center of the distribution.
4. The node-routing method developed for this study provides a convenient and accurate approximation to advective transport within single fractures.

The relatively small contribution of internal variability to field-scale transport is consistent with the previous results of /Painter and Cvetkovic 2001/ and lends further support for ignoring internal variability in geosphere-scale safety calculations.

These conclusions are based on the assumed model for single-fracture variability. Sensitivity studies described in this report suggest limited sensitivity to the assumed model. However, all of these sensitivity studies used a simple multi-gaussian random space function model because of limited information on internal aperture variability. More complicated models that include asperities or improved connectivity between large-aperture regions may lead to more channeling and smaller values of β.

An empirical post-processing of the β distribution similar to that used in Figure 3-3 is recommended to account for internal variability in future safety assessment calculations. The proposed procedure is to perform a limited number of small-scale DFN simulations with internal variability to obtain an empirical relationship between the β distributions with and without internal variability. This empirical transformation of the β distribution could then be applied to the results of large DFN simulations as a post-processing step. In the absence of additional information on internal variability, Equation 1 is recommended as the transformation. However, improved models of internal variability are expected to be available in the near future – as these become available, simulations like those in the report should be repeated to obtain an improved transformation.

References

Brown S R, 1995. Simple mathematical model of a rough fracture, Journal of Geophysical Research, 100(84), 5,941–5,922.

Cvetkovic V, Selroos J-O, Cheng H, 1999. Transport of reactive tracers in rock fractures, Journal of Fluid Mechanics, 378, 335–356.

Cvetkovic V, Painter S, Selroos J-O, Cheng H, 2004. Stochastic simulation of radionuclide migration in discretely fractured rock near the Aspo Hard Rock Laboratory, Water Resources Research 40, doi:10.1029/2003WR002655.

Desbarats A J, 1990. Macrodispersion in sand-shale sequences, Water Resources Research 26(1), 153–163.

Deutsch C V, Journel A G, 1992. GSLIB: Geostatistical Software Library and User's Guide, Oxford University Press, New York.

Doe T, 1993. Derivation of fracture transport aperture. Unpublished report. Golder Associates Inc., Seattle Washington USA.

Outters N, 2003. A generic study of discrete fracture network transport properties using FracMan/MAFIC, SKB R–03–13. Svensk Kärnbränslehantering AB.

Painter S, Cvetkovic V, Selroos J-O, 1998. Transport and retention in fractured rock: Consequences of a power-law distribution for fracture lengths, Physical Review E 57(6), 6,917–6,922.

Painter S, Cvetkovic V, 2001. Stochastic analysis of early tracer arrival in a segmented fracture pathway, Water Resources Research, 37(6), 1,669–1,680.

Painter S, 2003. Statistical analysis of discrete fracture network simulations, SKB TS-03-01. Svensk Kärnbränslehantering AB.

Painter S, Cvetkovic V, 2005. Upscaling discrete fracture network simulations: An alternative to continuum transport models, Water Resources Research, 41, doi:10.1029/2004WR003682.

Robinson B A, Li C, Ho C K, 2003. Performance assessment model development and analysis of radionuclide transport in the unsaturated zone, Yucca Mountain, Nevada, Journal of Contaminant Hydrology 62, 249–268.

Svensson U, 2001. A continuum representation of fracture networks. Part I: Method and basic test cases. Journal of Hydrology 250, 170–186.